Response of MicroRNAs to *In Vitro* Treatment with Graphene Oxide

Yiping Li,[†] Qiuli Wu,[†] Yunli Zhao,[†] Yunfei Bai,[‡] Pingsheng Chen,[†] Tian Xia,[§] and Dayong Wang[†,*]

[†]Key Laboratory of Developmental Genes and Human Diseases in Ministry of Education, Medical School of Southeast University, Nanjing 210009, China, [‡]State Key Laboratory of Bioelectronics, School of Biological Science & Medical Engineering, Southeast University, Nanjing 210096, China, and [§]Department of Medicine, Division of NanoMedicine, University of California, Los Angeles, California 90095, United States

ABSTRACT Graphene oxide (GO) can be potentially used in biomedical and nonbiomedical products. The *in vivo* studies have demonstrated that GO is predominantly deposited in the lung. In the present study, we employed SOLiD sequencing technique to investigate the molecular control of *in vitro* GO toxicity in GLC-82 pulmonary adenocarcinoma cells by microRNAs (miRNAs), a large class of short noncoding RNAs acting to post-transcriptionally inhibit gene expression. In GLC-82 cells, GO exposure at concentrations more than 50 mg/L resulted in severe reduction in cell viability, induction of lactate dehydrogenase leakage, reactive oxygen species production and apoptosis, and dysregulation of cell cycle. GO was localized in cytosol, mitochondria, endoplasmic reticulum, and nucleus of cells. Based on SOLiD sequencing, we identified 628 up-regulated and 25 down-regulated miRNAs in GO-exposed GLC-82 cells. Expression of some selected dysregulated miRNAs was concentration-dependent in GO-exposed GLC-82 cells. The dysregulated miRNAs and their predicted targeted genes were involved in many biological processes. By combining both information on targeted genes for dysregulated miRNAs and known signaling pathways for apoptosis control, we hypothesize that the dysregulated miRNAs could activate both a death receptor pathway by influencing functions of tumor necrosis factor α receptor and caspase-3 and a mitochondrial pathway by affecting functions of p53 and Bcl-2 in GO-exposed GLC-82 cells. Our results provide an important molecular basis at the miRNA level for explaining *in vitro* GO toxicity. Our data will be also useful for developing new strategies to reduce GO toxicity such as surface chemical modification.

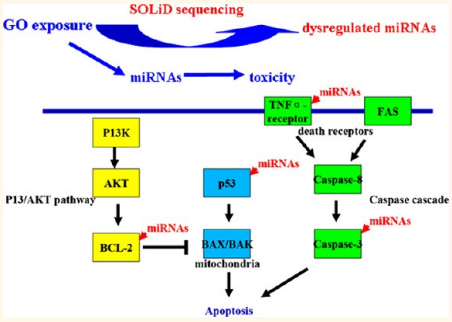

KEYWORDS: miRNAs · RNAomics · graphene oxide · *in vitro* toxicity · cell death

Graphene is a single-atom-thick, two-dimensional sheet of hexagonally arranged carbon atoms and has fascinating physical and chemical properties.[1] Graphene oxide (GO), extensively studied and applied in biomedical and nonbiomedical products, is one of the most important graphene derivatives.[2−4] Because of its physiologically stable property, GO was potentially used in delivery of anticancer drugs and genes, cell and tumor bioimaging, and photothermal therapy.[2−5] Nevertheless, there may still be a long way to go before realizing application of graphene family materials in clinical settings. One of the important obstacles is the potential toxicity of graphene and its derivatives in biological systems.[5]

The rapid development of nanotechnology increases the exposure levels of engineered nanomaterials (ENMs) for humans and the environment.[6−14] A number of groups have investigated the potential *in vitro* toxicity of GO to mammalian cells.[15−19] Low doses of GO did not induce an obvious cytotoxicity and cellular uptake in human pulmonary adenocarcinoma A549 cells and neuroblastoma SH-SY5Y cells; however, high doses of GO resulted in oxidative stress and caused reduction in viability of A549 or SH-SY5Y cells.[15,16] In HeLa cells, GO exhibited a dose-dependent toxicity and induced generation of reactive oxygen species (ROS).[17] GO showed a dose-dependent change of hemolytic activity in human red blood cells.[18] The cyto- and genotoxicities of GO to human stem cells were also size- and concentration-dependent.[19] Moreover, the GO nanosheet effectively inhibited growth of *Escherichia coli* bacteria.[20,21] The immunotoxicity of GO was determined in human immune cells such as dendritic cells, T lymphocytes, and macrophages.[22] The *in vivo* studies further demonstrated that GO was predominantly deposited in the lung for a long time with the difficulty of excretion.[23,24]

* Address correspondence to dayongw@seu.edu.cn.

Received for review August 29, 2013 and accepted February 10, 2014.

Published online February 10, 2014
10.1021/nn4065378

After intravenous injection, GO induced a high thrombogenicity and pulmonary edema and granuloma formation in the lung.[23−25] Mice treated intratracheally with GO induced severe and persistent lung injury, increase in the rate of mitochondrial respiration and ROS generation, and activation of inflammation and apoptosis.[26] With *Caenorhabditis elegans* as an *in vivo* assay system, the underlying chemical and cellular mechanisms of GO-induced toxicity have also been examined.[27,28]

Although the *in vitro* and *in vivo* studies have demonstrated the possible toxic effects of GO, so far, the underlying molecular mechanism for GO toxicity is still largely unclear. Yuan *et al.* performed an iTRAQ-coupled 2D LC-MS/MS proteome analysis on GO toxicity in human hepatoma HepG2 cells, and overall, 30 differentially expressed proteins involved in metabolic pathway, redox regulation, cytoskeleton formation, and cell growth were identified.[29] MicroRNAs (miRNAs), a large class of short noncoding RNAs found in many plants, animals, and humans, usually act to post-transcriptionally inhibit gene expression.[30] The SOLiD sequencing technique could be used to acquire the miRNA expression profiling in NIH/3T3 cells treated with Fe_2O_3 nanoparticles (Fe_2O_3 NPs), CdTe quantum dots (CdTe QDs), and multiwalled carbon nanotubes (MWCNTs).[31] In the present study, we employed the SOLiD sequencing technique to investigate the miRNA control of *in vitro* GO toxicity in pulmonary adenocarcinoma GLC-82 cells.[32] The data presented here will be useful for our understanding the molecular mechanism for formation and regulation of GO toxicity at the level of miRNA molecules.

RESULTS AND DISCUSSION

Physicochemical Properties of Prepared GO. GO, synthesized according to the modified Hummer's method,[33,34] was black and dispersed well. Transmission electron microscopy (TEM) and atomic force microscopy (AFM) images indicated the sheet-like shape of prepared GO (Figure 1a,b). The height image from AFM indicates that the thickness of the prepared GO was ~1.0 nm in topographic height, corresponding to approximately one layer (Figure 1b). After sonication, the TEM images of GO suggest that the size of GO aggregates in Roswell Park Memorial Institute (RPMI) was 423 ± 21 nm (Figure 1c). The average size of GO after sonication in RPMI medium was 51 nm (Figure 1d). Fourier transform infrared spectroscopy (FTIR) spectrum of GO showed that the peaks at 1401 and 3406 cm^{-1} were attributed to O−H stretching vibration, the peak at 1638 cm^{-1} is attributed to C═O stretching vibration, and the peak at 1036 cm^{-1} is attributed to vibration of C−O (alkoxy) (Figure 1e). Raman spectroscopy showed that the D-band signal was appeared after treatment with sulfuric acid and $KMnO_4$, indicating the introduction of disorder into the graphite layer (Figure 1f). Zeta-potential of GO in RPMI medium was measured by the Nano Zetasizer using a dynamic light scattering (DLS) technique, and the zeta-potential of GO in K medium was −22.8 mV. The sonicated GO was used for the further toxicity assessment.

***In Vitro* Localization of GO in GLC-82 Cells.** To investigate the *in vitro* distribution of GO, we performed the TEM to observe the distribution of GO in GLC-82 cells. In control GLC-82 cells without GO treatment, we could not detect the GO distribution in both the nucleus and the cytosol (Supporting Information Figure S1a). After exposure for 3 h, GO could be localized in both cytoplasm and nucleus (Figure 2a,b). In the nucleus, GO was mainly located in the border region (Figure 2a). In the cytoplasm, GO could be located in some of the mitochondria (Figure 2b). Moreover, after exposure for 72 h, a large amount of GO was deposited in both cytosol and nucleus (Figure 2c). In the nucleus, GO could be located at most of the regions including the border region (Figure 2c,d and Figure S1b). In the cytoplasm, GO could be located in both mitochondria and endoplasmic reticulum (Figure 2d,e).

***In Vitro* Toxicity of GO on GLC-82 Cells.** To determine the *in vitro* toxicity of GO in GLC-82 cells, we first performed the cell counting kit-8 (CCK-8) viability assay. On the basis of the microscopic observation, we found that GO could scatter inside the GLC-82 cells or aggregate outside the GLC-82 cells (Figure 3a). With the increase of GO exposure concentrations, morphology of most of the GO-exposed GLC-82 cells became round or irregular, had unclear cell boundary, floated in the media, or exhibited cell debris (Figure 3a). After exposure to different concentrations of GO, we further observed that the *in vitro* GO toxicity was both time- and concentration-dependent (Figure 3b). With the increase in exposure concentration or extension of exposure time, cell viability gradually decreased in GO-exposed GLC-82 cells (Figure 3b). Nevertheless, the cell viability in GLC-82 cells treated with 200 mg/L of GO for 72 h could remain at the level of approximately 58.7% (Figure 3b).

To examine the possible underlying mechanism for GO-induced decrease in cell viability, we investigated the effects of GO exposure on integrity of cell membrane as revealed by intracellular lactate dehydrogenase (LDH) assay. Exposure to the examined concentrations of GO for 48 h all induced the significant LDH leakage (Figure 3c). Because the intracellular LDH molecules would be released out of cells if the examined cell membrane is damaged, our data imply that GO exposure would cause the damage on membrane integrity in GLC-82 cells. Accompanied with the damage on cell membrane integrity, we further observed that exposure to 100 mg/L of GO for 48 h significantly induced the ROS production in GLC-82 cells (Figure 3d), implying the induction of oxidative stress in GO-exposed GLC-82 cells. Moreover, the flow cytometry (FCM) assay demonstrates that exposure to 100 mg/L

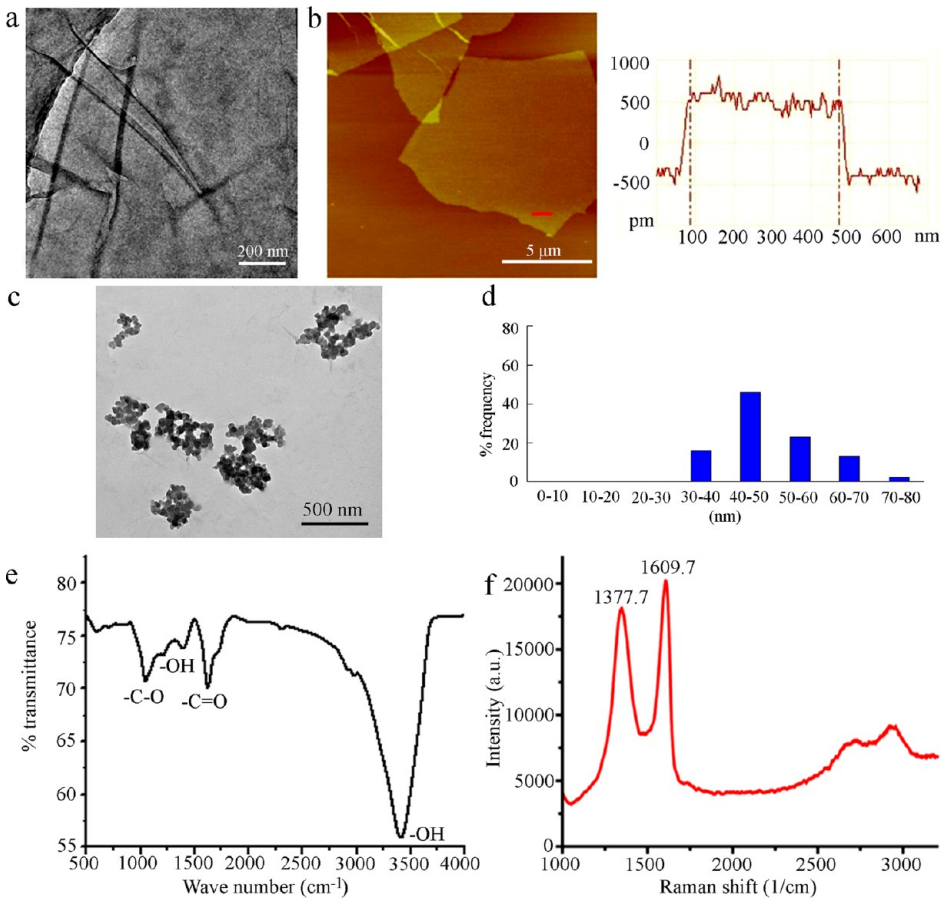

Figure 1. Physicochemical properties of prepared GO. (a) TEM image of GO before sonication. (b) AFM image of GO. (c) TEM image of GO in RPMI medium after sonication. (d) Size distribution of GO in RPMI medium after sonication. (e) FTIR spectrum of GO. (f) Raman spectrum of GO.

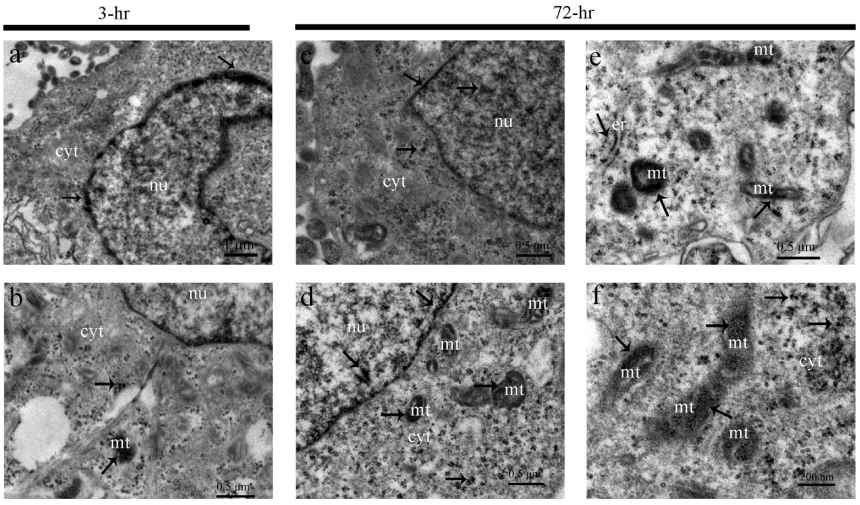

Figure 2. Localization of GO in GLC-82 cells. (a,b) TEM assay of GO localization in GLC-82 cells exposed to GO for 3 h. (c−f) TEM assay of GO localization in GLC-82 cells exposed to GO for 72 h: nu, nucleus; cyt, cytoplasm; mt, mitochondria; er, endoplasmic reticulum. The GO exposure concentration was 100 mg/L. Arrowheads indicate the localization of GO in GLC-82 cells.

of GO for 48 h significantly induced the apoptosis in GLC-82 cells (Figure 3e). The apoptosis rate in GLC-82 cells was approximately 22.7-fold that in control cells (Figure 3e). Meanwhile, GO exposure significantly increased the population of S-phase GLC-82 cells and decreased the population of G2-phase GLC-82 cells (Figure 3e), suggesting the alteration of cell cycle in GO-exposed GLC-82 cells.

MiRNA Participant in the Control of GO Cytotoxicity. To determine the possible involvement of miRNAs in

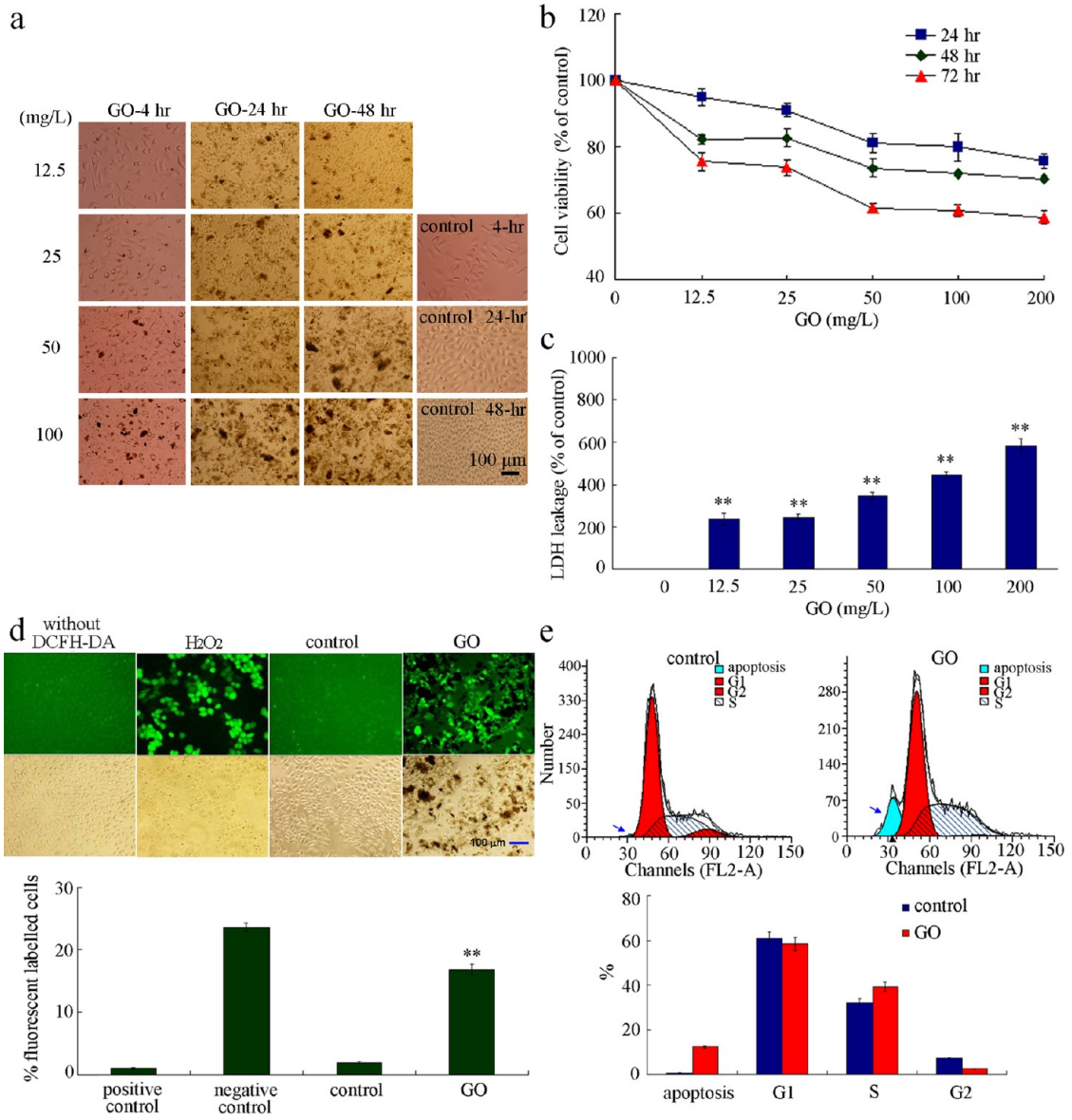

Figure 3. Toxicity of GO on GLC-82 cells. (a) Effect of GO on morphology of GLC-82 cells. The morphology of GLC-82 cells was examined based on CCK-8 assay after cells were treated with different concentrations of GO. (b) Effects of GO on cell viability of GLC-82 cells. Cell viability was examined based on CCK-8 assay after GLC-82 cells were treated with different concentrations of GO. (c) Effect of GO on membrane integrity of GLC-82 cells based on LDH assay. (d) ROS production in GLC-82 cells treated with 100 mg/L of GO for 48 h. The positive control was prepared by culturing the cells with RPMI-1640 containing 100 μM of H_2O_2 for 1 h prior to the addition of DCFH-DA. The cells without DCFH-DA treatment was taken as a negative control. The control means that cells without exposure to GO were labeled by the DCFH-DA. (e) Effects of 100 mg/L of GO exposure on apoptosis and cell cycle in GLC-82 cells based on FCM assay. Bars represent mean ± SEM, *$p < 0.05$, **$p < 0.01$.

controlling GO toxicity, the SOLiD sequencing, a method widely used for analysis of miRNA expression profiling,[31] was performed to compare the miRNA expression profiling between control and 100 mg/L of GO exposure. We performed a clustering analysis according to length and chromosome location for the detected miRNA sequences. The detected miRNA sequences appeared as the size of 14−26 nucleotides (Figure 4a), and among them, most SOLiD sequences were found to be distributed between 19 and 22 nucleotides, which were considered as mature miRNAs by subsequent miRNA database blasting (Figure 4a). The miRNAs detected in the SOLiD sequencing were located on all chromosomes including the sex chromosome X (Figure 4b). Most SOLiD sequences were localized onto chromosome 1, 19, or X (Figure 4b). These data imply the feasibility of RNAomics study and the possible participation of miRNAs in controlling GO cytotoxicity.

Dysregulated MiRNA Expression by GO Exposure. The dysregulated expression of miRNAs in GO-exposed GLC-82 cells was investigated with the fold-change analysis and developed for further analysis based on statistical significance and use of a 2.0-fold-change cutoff. Annotations of differentially expressed genes were acquired

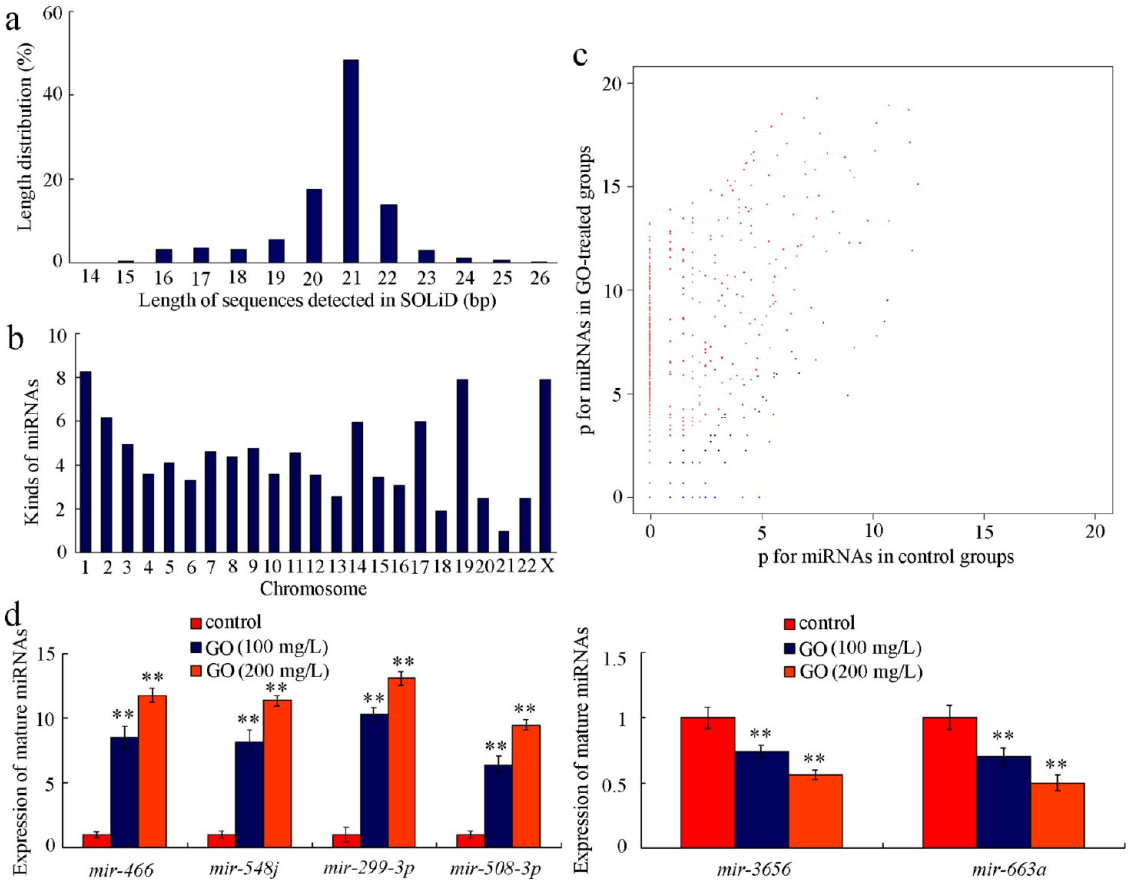

Figure 4. Results of SOLiD sequencing. (a) Length distribution of miRNAs detected from SOLiD sequencing. (b) Chromosome localization of miRNAs examined revealed by SOLiD sequencing. (c) Differential expression of miRNAs with *p* value analysis. (d) Expression pattern of mature miRNAs detected by real-time PCR after exposure to GO for 48 h. Bars represent mean ± SEM, **$p < 0.01$.

by comparing the miRNA sequences with the databases of Genbank and miRbase databases (Table S1, Figure 4c, and Figure S2). In the present study, we found 653 differentially expressed miRNAs (Table S1). Among these miRNAs, 628 up-regulated miRNAs and 25 down-regulated miRNAs were identified (Table S1, Figure 4c, and Figure S2). The differential expression of miRNAs with *p* value analysis suggested that the characteristic expression profiles existed in GO-exposed GLC-82 cells compared with that in control GLC-82 cells (Figure 4c). Therefore, the expression patterns of miRNAs were globally influenced by GO in GLC-82 cells.

Besides the SOLiD sequencing, we also randomly selected several candidate miRNAs and performed the quantitative analysis by real-time polymerase chain reaction (PCR). After exposure to 100 mg/L of GO for 48 h, expression levels of *mir-466*, *mir-548j*, *mir-299-3p*, and *mir-508-3p* were significantly increased, and expression levels of *mir-3656* and *mir-663a* were significantly decreased compared with control (Figure 4d). The expression patterns for these candidate miRNAs were similar to those from SOLiD sequencing (Table S1 and Figure 4d). Moreover, the miRNA expression was concentration-dependent in GO-exposed GLC-82 cells (Figure 4d).

Prediction of Targeted Genes for Dysregulated MiRNAs in GO-Exposed GLC-82 Cells and the Assessment of Gene ontology. Using the TargetScan database, we predicted the possible targeted genes for dysregulated miRNAs by $p < 0.05$ cutoff. We found 181 and 845 possible targeted genes for down- and up-regulated miRNAs, respectively. Gene ontology analysis provides the ontology of defined terms and gene product properties. Based on the dysregulated miRNA genes and their predicted targeted genes, the biological processes involved in the *in vitro* GO exposure were further evaluated by DESeq. Our data showed 89 up-regulated and 12 down-regulated gene ontology terms (Tables S2 and S3). The significantly influenced gene ontology terms were mainly classified into several categories, which at least contained biological processes of cell growth, cell cycle, cell death, inflammation, cell metabolism, vesicle transportation, development, and cell protection (Figure 5a,b and Tables S2 and S3).

Analysis of Signal Pathways Mediated by the Predicted Targeted Genes for Dysregulated MiRNAs in GO-Exposed GLC-82 Cells. To obtain comprehensive insight into the molecular basis of miRNAs differentially expressed in GO-exposed GLC-82 cells, we further employed the Kyoto Encyclopedia of Genes and Genomes (KEGG) pathway

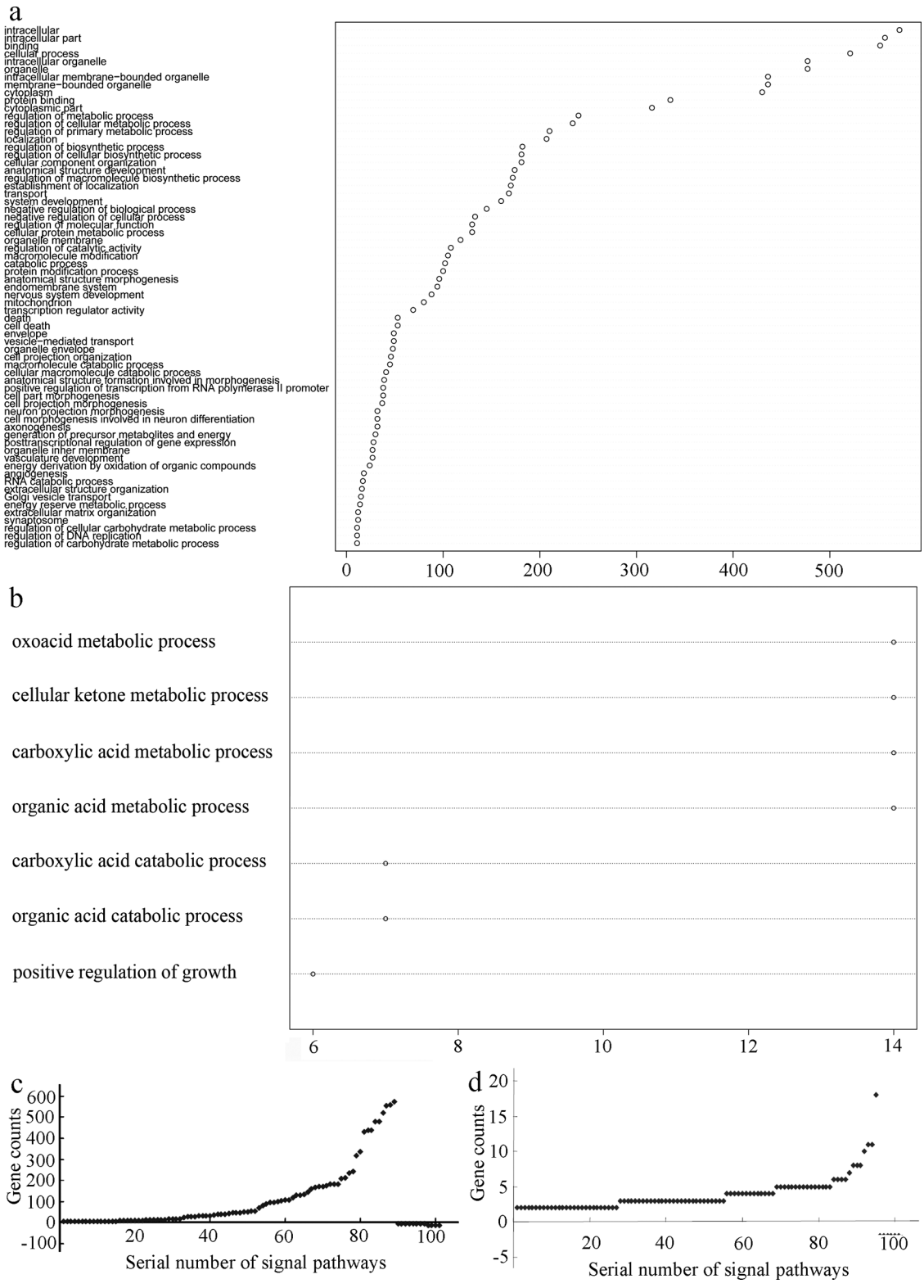

Figure 5. Assessment of gene ontology terms and signal pathways. (a) Gene ontology terms with gene counts more than 10 based on up-regulated miRNAs. (b) Gene ontology terms with gene counts more than 5 based on down-regulated miRNAs. (c) Predicted gene ontology terms based on differentially regulated miRNAs. (d) Predicted KEGG signal pathways based on differentially regulated miRNAs.

database to identify the related signal pathways mediated by the predicted targeted genes for dysregulated miRNAs in GO-exposed GLC-82 cells. KEGG pathway mapping is the process to map molecular data sets, especially large-scale data sets in genomics, and the related signaling pathways can be extracted by

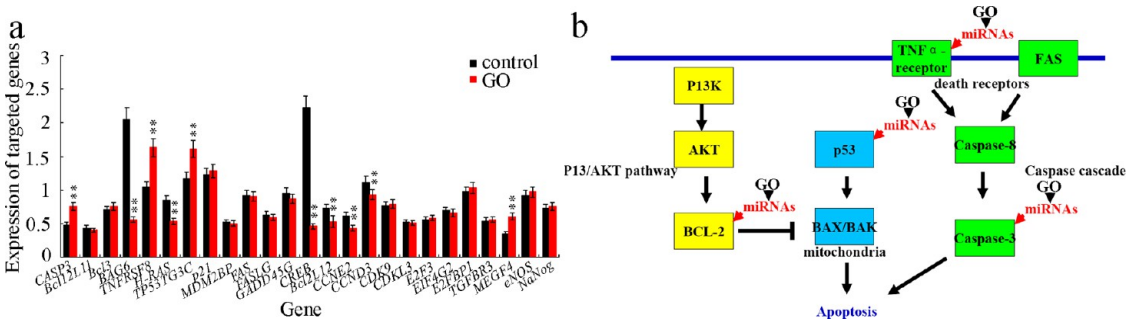

Figure 6. Expression of possible targeted genes for dysregulated miRNAs in GO-exposed GLC-82 cells. (a) Expression patterns of targeted genes for dysregulated miRNAs in GO-exposed GLC-82 cells. Bars represent mean ± SEM, $^{**}p < 0.01$. (b) Model for miRNAs in regulating the GO-induced apoptosis in GLC-82 cells. MiRNAs could regulate the GO-induced apoptosis by influencing both the death receptor pathway and the mitochondrial pathway in GLC-82 cells.

pathway mining tool. In the present study, we identified 98 up-regulated and 6 down-regulated signaling pathways (Tables S4 and S5 and Figure 5c,d). The activated signaling pathways possibly by GO exposure mainly focused on signaling pathways related to thrombosis, oxidative stress, inflammation, cell growth/proliferation, apoptosis, cell cycle, cell metabolism, membrane trafficking, development, stress response, and G-protein-coupled signaling pathway (Tables S4 and S5), which was largely consistent with the data from gene ontology.

Molecular Mechanism for Dysregulated MiRNAs in Regulating the *In Vitro* GO Toxicity. To determine the molecular mechanism for miRNAs in regulating *in vitro* GO toxicity, we searched the predicted targeted genes involved in the control of cell death or cell cycle for the dysregulated miRNAs in GLC-82 cells. We found that *CASP3*, *Bcl12L11*, *Bcl3*, *BAG6*, *TNFRSF8*, *H-RAS*, *TP53TG3C*, *p21*, *MDM2BP*, *FAS*, *FASLG*, *GADD45G*, *CREB*, *Bcl2L12*, *CCNE2*, *CCND3*, *CDK9*, *CDKL3*, *E2F3*, *E1F4G2*, *E2FBP1*, *TGFBR3*, *MEGF4*, *eNOS*, and *NaNog* genes were the possible targeted genes for the dysregulated miRNAs in GLC-82 cells, and these genes are involved in the molecular control of cell death and/or cell cycle (Table S6).[35−37] We further performed the quantitative analysis for these genes in control and GO-exposed GLC-82 cells by real-time PCR. Interestingly, we found that expression patterns of *CASP3*, *BAG6*, *TNFRSF8*, *H-RAS*, *TP53TG3C*, *CREB*, *Bcl2L12*, *CCNE2*, *CCND3*, and *MEGF4* genes were significantly altered in GLC-82 cells exposed to 100 mg/L of GO for 48 h compared with control (Figure 6a). After exposure to 100 mg/L of GO, expression levels of *CASP3*, *TNFRSF8*, *TP53TG3C*, and *MEGF4* genes were significantly increased, whereas expression levels of *BAG6*, *H-RAS*, *CREB*, *Bcl2L12*, *CCNE2*, and *CCND3* genes were significantly decreased in GLC-82 cells (Figure 6a). In humans, *CASP3* encodes a caspase-3 protein, *TNFRSF8* a tumor necrosis factor α (TNF α) receptor, *TP53TG3C* a TP53 target gene 3 protein, *MEGF4* a slit homologue 1 protein, *BAG6* a large proline-rich protein, *H-RAS* a GTPase HRas, *CREB* a cAMP responsive element binding protein, *Bcl2L12* a bcl-2-like protein, *CCNE2* a G1/S-specific cyclin-E2 protein, and *CCND3* a G1/S-specific cyclin-D3 protein (Table S6). The corresponding dysregulated miRNAs in GO-exposed GLC-82 cells for these differentially expressed genes are shown in Table S7.

In the present study, we provide the data to further support such a hypothesis that high concentrations of GO would cause oxidative stress and induce cell death.[15,16] In GLC-82 cells, exposure to GO at concentrations more than 50 mg/L resulted in severe reduction in cell viability and induction of LDH leakage (Figure 3b,c). For the cellular mechanism of *in vitro* GO toxicity in GLC82 cells, we raise two possibilities. One possibility was the activation of oxidative stress, and another possibility was the induction of apoptosis and the dysregulation of cell cycle (Figure 3d,e). Thus, the concentrations of pristine GO for drug delivery should be carefully considered.

In GLC-82 cells, we found that GO was localized in cytosol, mitochondria, endoplasmic reticulum, and nucleus (Figure 3), which is largely consistent with the observations in other assay systems such as *C. elegans* and human fibroblast cells.[23,28] GO could be localized in mitochondria of intestinal cells of *C. elegans* and human fibroblast cells.[23,28] Different from the observations in human fibroblast cells and intestinal cells of nematodes, some of the GO could also be found to be located in the nucleus and endoplasmic reticulum in GLC-82 cells (Figure 3). Previous studies have demonstrated that some of the ENMs can be translocated into the nucleus from the cytosol.[38−41] One of the important mechanisms for the translocation of ENMs into nucleus is through the nuclear pore complexes (NPCs) with a central channel up to 40 nm.[38−41] Another mechanism for translocation of ENMs into the nucleus is the mitotic partitioning.[38] Our data suggest that GO was first accumulated along the border of the nucleus and then gradually accumulated inside the nucleus (Figure 2), which implies that at least one of the possibilities for GO to be translocated into the nucleus may be through the NPCs. The size (approximately 51 nm) of GO in the examined medium

further suggest that GO in the cytosol has the possibility to be adjusted into a particle with a size less than 40 nm and then to be translocated into the nucleus of GLC-82 cells through the NPCs.

So far, there is a huge knowledge gap between the use of GO and the prediction of possible health risks. That is, we still know little about the molecular mechanism for toxicity formation from GO. Previous study identified 30 differentially expressed proteins involved in several biological aspects in GO-exposed human hepatoma HepG2 cells with the aid of iTRAQ-coupled 2D LC-MS/MS proteome analysis.[29] In organisms, miRNAs are repressors of gene expression at the transcription level and widely participate in both physiological and pathological processes.[30] In the present study, we performed the systematic investigation on miRNA control of *in vitro* GO toxicity with the aid of SOLiD sequencing technique. The reason for selecting GLC-82 cells as the *in vitro* assay system is that GO is predominantly deposited in the lung of animals after exposure.[23,24] On the basis of SOLiD sequencing, we identified 628 up-regulated and 25 down-regulated miRNAs in GO-exposed GLC-82 cells (Table S1 and Figure 4c). Expression of some selected dysregulated miRNAs was concentration-dependent in GO-exposed GLC-82 cells (Figure 4d). Moreover, these dysregulated miRNAs may be involved in many biological aspects including cell growth, cell cycle, cell death, inflammation, cell metabolism, vesicle transportation, development, and cell protection in GO-exposed GLC-82 cells (Figure 5a,b and Tables S2 and S3). Correspondingly, based on the KEGG pathway mapping for possible targeted genes of dysregulated miRNAs, GO-activated signaling pathways were involved in thromobosis, oxidative stress, inflammation, cell growth/proliferation, apoptosis, cell cycle, cell metabolism, membrane trafficking, development, stress response, and G-protein-coupled signaling pathway in GLC-82 cells (Tables S4 and S5). These results provide a systematically molecular basis at the miRNA level for explaining the GO toxicity formation in lung cells.

Especially, by combining both the predicted targeted genes for dysregulated miRNAs in GO-exposed GLC-82 cells and the known signaling pathway for apoptosis control, we raise a model for miRNA control of GO-induced apoptosis (Figure 6b). There are two fundamental pathways for apoptosis control: the death receptor pathway and the mitochondrial pathway.[35−37] The death receptor pathway is initiated by cell surface receptor-mediated activation of caspases, a family of cysteine proteases, and the mitochondrial pathway involves both the P13/AKT-activated Bcl-2 family and p53 signal.[35−37] In GO-exposed GLC-82 cells, the dysregulated miRNAs could activate the death receptor pathway by influencing the functions of tumor necrosis factor α (TNFα) receptor and caspase-3 (Figure 6b). Moreover, the dysregulated miRNAs could activate the mitochondrial pathway by affecting the functions of p53 and Bcl-2 in GO-exposed GLC-82 cells (Figure 6b). Therefore, miRNAs could regulate the GO-induced apoptosis by influencing both the death receptor pathway and the mitochondrial pathway in GLC-82 cells. Besides these, BAG6 can also mediate cell death by forming a complex with UBL4A and GET4.[42] The oncogenic H-Ras can induce DNA damage and subsequent senescence.[43]

Furthermore, some of the examined genes regulated by dysregulated miRNAs in GLC-82 cells are also involved in cell cycle control. For example, *p53* can negatively regulate the activity of cyclin D.[36] *CCND3*, a cyclin D gene, and *CCNE2*, a cyclin E gene, activate cyclin-dependent kinases.[44,45] *MEGF4* is involved in the induction of cell proliferation.[46] CREB regulates the cell cycle arrest in cancer cells.[47]

CONCLUSION

In summary, in the present study, we performed the systematic investigation on miRNA response to the *in vitro* GO exposure using GLC-82 cells as the assay system. Our data here provide an important basis for our further understanding the molecular mechanism at the miRNA level for GO toxicity formation. The identified dysregulated miRNAs in GLC-82 cells may serve as the potential biomarkers for assessing the GO toxicity. Moreover, although the pristine graphene and GO tend to be toxic in a dose-dependent manner, the functionalized nano-GO exhibits a much reduced *in vitro* and *in vivo* toxicity.[5,26,48−51] Considering the potential of the graphene family in medical applications,[52,53] the obtained knowledge here will also be useful for guaranteeing the future development of related safe nanotechnologies associated with the graphene family by specific surface chemical modifications.

EXPERIMENTAL SECTION

Reagents and Preparation of GO. GO was prepared from the natural graphite powder by a modified Hummer's method.[33,34] Graphite (2 g) and sodium nitrate (1 g) were added to a 250 mL flask, and then the concentrated H_2SO_4 (50 mL) was slowly added with stirring on ice. After being stirred for 30 min, $KMnO_4$ (7 g) was added to the mixture over 1 h, and 90 mL of H_2O was slowly dripped to cause an increase in temperature to 70 °C after the temperature of the mixture warmed to 35 °C. Diluted suspension was stirred at 70 °C for another 15 min and further treated with a mixture of 7 mL of 30% H_2O_2 and 55 mL of H_2O. The resulting warm suspension was filtered to result in a yellow-brown filter cake, which was washed with a solution of 3% HCl, followed by drying at 40 °C for 24 h. Finally, GO was obtained by ultrasonication of as-made graphite oxide in water for 1 h.

Characterization of GO. Prepared GO materials were characterized by TEM (JEM-200CX, JEOL, Japan), AFM (SPM-9600, Shimadzu, Japan), FTIR (Avatar 370, Thermo Nicolet, USA), Raman spectroscopy (Renishaw Invia Plus laser Raman spectrometer, Renishaw, UK), and Nano Zetasizer (Malvern Instrument Ltd. UK). TEM images were collected on the field emission JEM-200CX transmission electron microscopy, equipped with a CCD camera. A few drops of the GO suspension solution were deposited on the TEM grid, dried, and evacuated before analysis. To perform AFM measurement, GO suspension solutions were pipetted on Si substrates, and substrates were air-dried and placed directly under the AFM tip. Zeta-potential was analyzed by Nano Zetasizer using a DLS technique.

GLC-82 Cell Line. GLC-82 is one specific lung cancer cell line, which was established from the cancerous tissue in a female patient with pulmonary adenocarcioma from a high lung cancer incidence area (Gejiu, China).[32] The etiology of lung cancer in Gejiu was closely associated with radiation of radon, arsenic, and industrial dust, which partly imitated the malignant transformation induced by chemical substances in normal cells.[32] The cells were grown in RPMI-1640 medium (GIBCO, BRL, USA) supplemented with 10% (v/v) fetal bovine serum (FBS) (GIBCO, BRL, USA) and antibiotics (100 U/mL streptomycin and 100 U/mL penicillin) at 37 °C in a humidified incubator with 5% CO_2. The freshly prepared medium was replaced every day. The confluent cells were harvested with 0.25% trypsin-ethylene diamine tetraacetic acid (EDTA) solution.

GO Suspension Preparation and Exposure. GO was dispersed in sterilized deionzied water to prepare the stock solution (1.0 mg/mL). Stock solution was sonicated for 30 min (40 kHz, 100 W) and diluted to different concentrations (12.5, 25, 50, 100, and 200 mg/L) with RPMI-1640 medium just prior to exposure. RPMI-1640 medium was used as a control. All the other chemicals were obtained from Sigma-Aldrich (St. Louis, MO, USA).

Distribution of GO. To examine the distribution of GO in GLC-82 lung cancer cells by TEM, GLC-82 cells were plated in 6-well plates and cultured overnight and then treated with GO (100 mg/L). GLC-82 cells were collected and washed twice with phosphate buffer saline (PBS) buffer and fixed with 2.5% glutaraldehyde and 1% osmium tetroxide. The fixed cells were dehydrated through graded ethanol, washed, and embedded in Epon/Araldite resin. Serial sections were collected using an Ultracut E microtome. Images were obtained on an electron microscope (JEM-200CX, JEOL, Japan).

CCK-8 Assay. The CCK-8 assay was used to evaluate cell viability. GLC-82 cells were seeded in 96-well plates (5×10^3 cells per well) and grown overnight, and then incubated with GO. After 24, 48, or 72 h incubation, the cells were washed with D-Hank's buffer, and 200 μL of WST-8 solution (Dojindo Molecular Technologies, Inc., USA) was introduced to each well to incubate for an additional 3 h at 37 °C. The optical density (OD) of each well at 450 nm was examined on a microplate reader (Thermo, Varioskan Flash).

LDH Activity Assay. Cell membrane integrity was analyzed by measuring the release of LDH with an LDH assay kit (Nanjing Jiancheng Bioengineering Institute, China). GLC-82 cells were plated in 96-well plates (5×10^3 cells per well) and cultured overnight, and then incubated with GO for 48 h. The absorbance at 490 nm was recorded on a microplate reader (Thermo, Varioskan Flash) and normalized by protein concentrations. The LDH release (% of control) is presented as the percentage of $(OD_{test} - OD_{blank})/(OD_{control} - OD_{blank})$, where OD_{test} is for the cells treated with GO, $OD_{control}$ is for the control sample, and OD_{blank} is for the wells without cells.

Assay of ROS Production. 2′,7′-Dichlorofluorescein diacetate (DCFH-DA) (Nanjing Jiancheng Bioengineering Institute, China), an oxidant-sensitive dye, was employed for ROS detection. GLC-82 cells were plated in 96-well plates (5×10^3 cells per well) and cultured overnight, and then exposed to GO (100 mg/L) for 48 h. The positive control was prepared by culturing the cells with RPMI-1640 containing 100 μM of H_2O_2 for 1 h prior to the addition of DCFH-DA. The ROS was detected by 20 μM of DCFH-DA labeling. The cells without DCFH-DA treatment were taken as a negative control. After 1 h labeling, the cells were washed with D-Hank's buffer three times, and the cells were observed and images taken by a fluorescence microscope. All of the procedures were performed in the dark. The DCFH-DA-labeled cells were further counted, and the percentage of positive cells was calculated. For each treatment, we took at least five pictures in different areas for counting positive cells and calculating the percentage of positive cells.

FCM Assay. GLC-82 cells were plated in 6-well plates and cultured overnight, and then exposed to GO (100 mg/L) for 48 h. After being washed twice by PBS buffer, the cells were fixed with 70% ethanol and stained with propidium iodide (PI) (100 mg/L). DNA indices for the cell cycle were monitored using a standard method from Becton Dickson FACS (BD Biosciences, San Jose, CA). Each histogram represented 10 000−100 000 cells for measurement of the DNA index. Histogram analysis was performed using a CellQuest program (BD Biosciences). We counted the sub-G0/G1 peak in the hypodiploid distribution below a DNA index of 1 ($<2n$). Based on the forward light scatter and PI fluorescence, apoptotic nuclei were identified as a hypodiploid DNA peak and were distinguished from cell debris.

Small RNA Extraction and SOLiD Sequencing. The cells were seeded on 35 mm dishes and cultured overnight, and then exposed to GO (100 mg/L) for 48 h to harvest with trypsin−EDTA. After being washed, the cells were lysed to extract small RNA for RNAomics assay. Briefly, the small RNAs were extracted according to the manufacturer's instructions from the mirVana miRNA isolation kit (Ambion) and converted into a double-stranded cDNA library followed by the adaptor ligation. The quality of library was performed by Agilent 2100 bioanalyzer after gel purification with Qiagen MinElute reaction cleanup kit and gel extraction kit. The double-stranded cDNA library was compatible with the Applied Biosystems SOLiD system for the next-generation high-throughput sequencing. The results of SOLiD developed by ABI could be in the form of nucleotide sequences and their coverage. By comparing those sequences with the databases of Genbank (www.ncbi.nlm.nih.gov/Genbank) and miRNAbase (http://www.mirbase.org), registered miRNAs could be determined from all the detected sequences.

Bioinformatics Analysis. The dysregulated expression of miRNAs in the GO-treated GLC-82 cells was analyzed by DESeq (an R package, a powerful tool to estimate the variance and test for differential expression). The data were extracted as up- or down-regulated miRNAs according to a cutoff of 2-fold change and were presented in the scatter diagram after normalization. The predicted targeted genes of miRNA significantly influenced by GO treatment were analyzed by TargetScan database (http://www.targetscan.org). Subsequently, to deeply exploit the possible molecular mechanisms involved, the predicted targeted genes prominently affected were enriched to both the gene ontology biological processes and the KEGG pathways through bioinformatics approaches (http://www.geneontology.org and http://www.genome.jp/kegg/) to be presented as gene ontology terms (GO terms) and signal pathways, respectively.

Reverse Transcription and Quantitative Real-Time PCR. Total RNA was isolated from cells using Trizol (Invitrogen, UK) according to the manufacturer's protocols. The purities and concentrations of RNA were evaluated by OD 260/280 in a spectrophotometer. cDNA synthesis was performed in a 12.5 μL reaction volume containing 625 ng total RNA, 0.5 mM reverse-transcript primers, 50 mM Tris-HCl, 75 mM KCl, 3 mM $MgCl_2$, 10 mM dithiothreitol, 20 units of ribonuclease inhibitor and 100 U of reverse transcriptase (Takara, China). After incubation at 25 °C for 5 min and 42 °C for 60 min, reverse transcriptase was inactivated at 70 °C for 15 min, and cDNAs were stored at 4 °C for further real-time PCR. After the cDNA synthesis, the relative expression levels were determined by real-time PCR in an ABI 7500 real-time PCR system with Evagreen (Biotium, USA). All reactions were performed in triplicate with the same cDNA samples. All reactions were performed in 10 μL reaction volume including cDNA and primers. PCR was processed with the following cycles: a 10 min activation and denaturation step at 95 °C, followed by 40 cycles of 15 s at 95 °C and 60 s at 60 °C. The primer information is shown in Tables S8−S10.

Statistical Analysis. All data were presented as mean ± standard error of the mean (SEM). Graphs were generated using Microsoft Excel (Microsoft Corp., Redmond, WA). Statistical

analysis was performed using SPSS 12.0 (SPSS Inc., Chicago, USA). Differences between groups were determined using analysis of variance (ANOVA). Probability levels of 0.05 and 0.01 were considered to be statistically significant.

Conflict of Interest: The authors declare no competing financial interest.

Acknowledgment. We thank D. Zhang for providing the GLC-82 cell line. This work was supported by grants from National Basic Research Program of China (No. 2011CB933404), and National Natural Science Foundation of China (Nos. 81172698 and 81202233).

Supporting Information Available: Additional figures of GO localization, miRNA expression analysis, and tables of differentially expressed miRNAs, gene ontology terms, signal pathways with gene counts, and designed primers. This material is available free of charge *via* the Internet at http://pubs.acs.org.

REFERENCES AND NOTES

1. Geim, A. K. Graphene: Status and Prospects. *Science* **2009**, *324*, 1530–1534.
2. Liu, Z.; Robinson, J. T.; Sun, X.; Dai, H. PEGylated Nanographene Oxide for Delivery of Water-Insoluble Cancer Drugs. *J. Am. Chem. Soc.* **2008**, *130*, 10876–10877.
3. Zhang, L.; Xia, J.; Zhao, Q.; Liu, L.; Zhang, Z. Functional Grapheme Oxide as a Nanocarrier for Controlled Loading and Targeted Delivery of Mixed Anticancer Drugs. *Small* **2010**, *6*, 537–544.
4. Shi, Z.; Gong, H.; Li, Y.; Wang, C.; Cheng, L.; Liu, Z. Graphene-Based Magnetic Plasmonic Nanocomposite for Dual Bioimaging and Photothermal Therapy. *Biomaterials* **2013**, *34*, 4786–4793.
5. Yang, K.; Li, Y.; Tan, X.; Peng, R.; Liu, Z. Behavior and Toxicity of Graphene and Its Functionalized Derivatives in Biological Systems. *Small* **2013**, *9*, 1492–1503.
6. Nel, A.; Xia, T.; Madler, L.; Li, N. Toxic Potential of Materials at the Nanolevel. *Science* **2006**, *311*, 622–627.
7. Xia, T.; Li, N.; Nel, A. E. Potential Health Impact of Nanoparticles. *Annu. Rev. Public Health* **2009**, *30*, 137–150.
8. Zhao, Y.-L.; Wu, Q.-L.; Li, Y.-P.; Wang, D.-Y. Translocation, Transfer, and *In Vivo* Safety Evaluation of Engineered Nanomaterials in the Non-Mammalian Alternative Toxicity Assay Model of Nematode *Caenorhabditis elegans*. *RSC Adv.* **2013**, *3*, 5741–5757.
9. Wu, Q.-L.; Li, Y.-P.; Tang, M.; Wang, D.-Y. Evaluation of Environmental Safety Concentrations of DMSA Coated Fe_2O_3-NPs Using Different Assay Systems in Nematode *Caenorhabditis elegans*. *PLoS ONE* **2012**, *7*, e43729.
10. Li, Y.-X.; Yu, S.-H.; Wu, Q.-L.; Tang, M.; Pu, Y.-P.; Wang, D.-Y. Chronic Al_2O_3-Nanoparticle Exposure Causes Neurotoxic Effects on Locomotion Behaviors by Inducing Severe ROS Production and Disruption of ROS Defense Mechanisms in Nematode *Caenorhabditis elegans*. *J. Hazard. Mater.* **2012**, *219*−*220*, 221–230.
11. Li, Y.-X.; Yu, S.-H.; Wu, Q.-L.; Tang, M.; Wang, D.-Y. Transmissions of Serotonin, Dopamine and Glutamate Are Required for the Formation of Neurotoxicity from Al_2O_3-NPs in Nematode *Caenorhabditis elegans*. *Nanotoxicology* **2013**, *7*, 1004–1013.
12. Wu, Q.-L.; Wang, W.; Li, Y.-X.; Li, Y.-P.; Ye, B.-P.; Tang, M.; Wang, D.-Y. Small Sizes of TiO_2-NPs Exhibit Adverse Effects at Predicted Environmental Relevant Concentrations on Nematodes in a Modified Chronic Toxicity Assay System. *J. Hazard. Mater.* **2012**, *243*, 161–168.
13. Zhao, Y.-L.; Wu, Q.-L.; Tang, M.; Wang, D.-Y. The *In Vivo* Underlying Mechanism for Recovery Response Formation in Nano-Titanium Dioxide Exposed *Caenorhabditis elegans* after Transfer to the Normal Condition. *Nanomedicine* **2014**, *10*, 89–98.
14. Nouara, A.; Wu, Q.-L.; Li, Y.-X.; Tang, M.; Wang, H.-F.; Zhao, Y.-L.; Wang, D.-Y. Carboxylic Acid Functionalization Prevents the Translocation of Multi-Walled Carbon Nanotubes at Predicted Environmental Relevant Concentrations into Targeted Organs of Nematode *Caenorhabditis elegans*. *Nanoscale* **2013**, *5*, 6088–6096.
15. Chang, Y.; Yang, S.; Liu, J.; Dong, E.; Wang, Y.; Cao, A.; Liu, Y.; Wang, H. *In Vitro* Toxicity Evaluation of Grapheme Oxide on A549 Cells. *Toxicol. Lett.* **2011**, *200*, 201–210.
16. Lv, M.; Zhang, Y.; Liang, L.; Wei, M.; Hu, W.; Li, X.; Huang, Q. Effect of Graphene Oxide on Undifferentiated and Retinoic Acid-Differentiaed SH-SY5Y Cells Line. *Nanoscale* **2012**, *4*, 3861–3866.
17. Zhang, X.; Hu, W.; Li, J.; Tao, L.; Wei, Y. A Comparative Study of Cellular Uptake and Cytotoxicity of Multi-Walled Carbon Nanotubes, Graphene Oxide, and Nanodiamond. *Toxicol. Res.* **2012**, *1*, 62–68.
18. Liao, K.; Lin, Y.; Macosko, C. W.; Haynes, C. L. Cytotoxicity of Graphene Oxide and Graphene in Human Erythrocytes and Skin Fibroblasts. *ACS Appl. Mater. Interfaces* **2011**, *3*, 2607–2615.
19. Akhavan, O.; Ghaderi, E.; Akhavan, A. Size-Dependent Genotoxicity of Graphene Nanoplatelets in Human Stem Cells. *Biomaterials* **2012**, *33*, 8017–8025.
20. Hu, W.; Peng, C.; Luo, W.; Lv, M.; LI, X.; Li, D.; Huang, Q.; Fan, C. Graphene-Based Antibacterial Paper. *ACS Nano* **2010**, *4*, 4317–4323.
21. Li, C.; Wang, X.; Chen, F.; Zhang, C.; Zhi, X.; Wang, K.; Cui, D. The Antifungal Activity of Graphene Oxide-Sliver Nanocomposites. *Biomaterials* **2013**, *34*, 3882–3890.
22. Zhi, X.; Fang, H.; Bao, C.; Shen, G.; Zhang, J.; Wang, K.; Guo, S.; Wan, T.; Cui, D. The Immunotoxicity of Graphenen Oxides and the Effects of PVP-Coating. *Biomaterials* **2013**, *34*, 5254–5261.
23. Wang, K.; Ruan, J.; Song, H.; Zhang, J.; Wo, Y.; Guo, S.; Cui, D. Biocompatibility of Grapgene Oxide. *Nanoscale Res. Lett.* **2011**, *6*, 8.
24. Zhang, X.; Yin, J.; Peng, C.; Hu, W.; Zhu, Z.; Li, W.; Fan, C.; Huang, Q. Distribution and Biocompatibility Studies of Grapheme Oxide in Mice after Intravenous Administration. *Carbon* **2011**, *49*, 986–995.
25. Singh, S. K.; Singh, M. K.; Nayak, M. K.; Kumari, S.; Shrivastava, S.; Gracio, J. J. A.; Dash, D. Thrombus Inducing Property of Atomically Thin Graphene Oxide Sheets. *ACS Nano* **2011**, *5*, 4987–4996.
26. Duch, M. C.; Budinger, G. R. S.; Liang, Y. T.; Soberanes, S.; Urich, D.; Chiarella, S. E.; Campochiaro, L. A.; Gongzalez, A.; Chandel, N. S.; Hersam, M. C.; *et al.* Minimizing Oxidation and Stable Nanoscale Dispersion Improves the Biocompatibility of Grapheme in the Lung. *Nano Lett.* **2011**, *11*, 5201–5207.
27. Zhang, W.; Wang, C.; Li, Z.; Lu, Z.; Li, Y.; Yin, J.; Zhou, Y.; Gao, X.; Fang, Y.; Nie, G.; *et al.* Unraveling Stress-Induced Toxicity Properties of Graphene Oxide and the Underlying Mechanism. *Adv. Mater.* **2012**, *24*, 5391–5397.
28. Wu, Q.-L.; Yin, L.; Li, X.; Tang, M.; Zhang, T.; Wang, D.-Y. Contributions of Altered Permeability of Intestinal Barrier and Defecation Behavior to Toxicity Formation from Graphene Oxide in Nematode *Caenorhabditis elegans*. *Nanoscale* **2013**, *5*, 9934–9943.
29. Yuan, J.; Gao, H.; Sui, J.; Duan, H.; Chen, W. N.; Ching, C. B. Cytotoxicity Evuluation of Oxidized Single-Walled Carbon Nanotubes and Graphene Oxide on Human Hepatoma HepG2 Cells: An iTRAQ-Coupled 2D LC-MS/MS Proteome Analysis. *Toxicol. Sci.* **2012**, *126*, 149–161.
30. Bartel, D. P. MicroRNAs: Genomics, Biogenesis, Mechanism, and Function. *Cell* **2004**, *116*, 281–297.
31. Li, S.; Wang, H.; Qi, Y.; Tu, J.; Bai, Y.; Tian, T.; Huang, N.; Wang, Y.; Xiong, F.; Lu, Z.; *et al.* Assessment of Nanomaterial Cytotoxicity with SOLiD Sequencing-Based MicroRNA Expression Profiling. *Biomaterials* **2011**, *32*, 9021–9030.
32. Wang, G.; Ye, Y.; Yang, X.; Liao, H.; Zhao, C.; Liang, S. Expression-Based *In Silico* Screening of Candidate Therapeutic Compounds for Lung Adenocarcinoma. *PLoS ONE* **2011**, *6*, e14573.
33. Hummers, W. S., Jr.; Offerman, R. E. Preparation of Graphite Oxide. *J. Am. Chem. Soc.* **1958**, *80*, 1339.
34. Kovtyukhova, N. I.; Olivier, P. J.; Martin, B. R.; Mallouk, T. E.; Chizhik, S. A.; Buzaneva, E. V.; Gorchinskiy, A. D. Layer-by-Layer Assembly of Ultrathin Composite Films from

Micron-Sized Graphite Oxide Sheets and Polycations. *Chem. Mater.* **1999**, *11*, 771–778.
35. Shortt, J.; Johnstone, R. W. Oncogenesis in Cell Survival and Cell Death. *Cold Spring Harbor Perspect. Biol.* **2012**, *4*, a009829.
36. Singhal, S.; Vachani, A.; Antin-Ozerkis, D.; Kaiser, L. R.; Albelda, S. M. Prognostic Implications of Cell Cycle, Apoptosis, and Angiogenesis Biomarkers in Non-Small Cell Lung Cancer: A Review. *Clin. Cancer Res.* **2005**, *11*, 3974–3986.
37. Malumbres, M.; Barbacid, M. Cell Cycle, CDKs and Cancer: A Changing Paradigm. *Nat. Rev. Cancer* **2009**, *9*, 153–166.
38. Symens, N.; Soenen, S. J.; Rejman, J.; Braeckmans, K.; De Smedt, S. C.; Remaut, K. Intracellular Partitioning of Cell Organelles and Extraneous Nanoparticles during Mitosis. *Adv. Drug Delivery Rev.* **2012**, *64*, 78–94.
39. Raoof, M.; Mackeyev, Y.; Cheney, M. A.; Wilson, L. J.; Curley, S. A. Internalization of C60 Fullerenes into Cancer Cells with Accumulation in the Nucleus *via* the Nuclear Pore Complex. *Biomaterials* **2012**, *33*, 2952–2960.
40. Fan, Y.; Li, C.; Cao, H.; Li, F.; Chen, D. The Intranuclear Rrelease of a Potential Anticancer Drug from Small Nanoparticles That Are Derived from Intracellular Dissociation of Large Nanoparticles. *Biomaterials* **2012**, *33*, 4220–4228.
41. Kim, J.; Izadyar, A.; Nioradze, N.; Amemiya, S. Nanoscale Mechanism of Molecular Transport through the Nuclear Pore Complex As Studied by Scanning Electrochemical Microscopy. *J. Am. Chem. Soc.* **2013**, *135*, 2321–2329.
42. Krenciute, G.; Liu, S.; Yucer, N.; Shi, Y.; Ortiz, P.; Liu, Q.; Kim, B. J.; Odejimi, A. O.; Leng, M.; Qin, J.; *et al.* Nuclear BAG6-UBL4A-GET4 Complex Mediates DNA Damage Signaling and Cell Death. *J. Biol. Chem.* **2013**, *288*, 20547–20557.
43. Weyemi, U.; Lagente-Chevallier, O.; Boufraqech, M.; Prenois, F.; Courtin, F.; Caillou, B.; Talbot, M.; Dardalhon, M.; Al Ghuzlan, A.; Bidart, J. M.; *et al.* ROS-Generating NADPH Oxidase NOX4 Is a Critical Mediator in Oncogenic H-Ras-Induced DNA Damage and Subsequent Senescence. *Oncogene* **2012**, *31*, 1117–1129.
44. Buschges, R.; Weber, R. G.; Actor, B.; Lichter, P.; Collins, V. P.; Reifenberger, G. Amplification and Expression of Cyclin D Genes (CCND1, CCND2 and CCND3) in Human Malignant Gliomas. *Brain Pathol.* **1999**, *9*, 435–442.
45. Caldon, C. E.; Sergio, C. M.; Burgess, A.; Deans, A. J.; Sutherland, R. L.; Musgrove, E. A. Cyclin E2 Induces Genomic Instability by Mechanisms Distinct from Cyclin E1. *Cell Cycle* **2013**, *12*, 606–617.
46. Lembach, K. J. Induction of Human Fibroblast Proliferation by Epidermal Growth Factor (EGF): Enhancement by an EGF-Binding Arginine Esterase and by Ascorbate. *Proc. Natl. Acad. Sci. U.S.A.* **1976**, *73*, 183–187.
47. Wang, P.; Huang, S.; Wang, F.; Ren, Y.; Hehir, M.; Wang, X.; Cai, J. Cyclic AMP-Response Element Regulated Cell Cycle Arrests in Cancer Cells. *PLoS ONE* **2013**, *8*, e65661.
48. Wojtoniszak, M.; Chen, X.; Kalenczuk, R. J.; Wajda, A.; Lapczuk, J.; Kurzewski, M.; Drozdzik, M.; Chu, P. K.; Borowiak-Palen, E. Synthesis, Dispersion, and Cytocompatibility of Graphene Oxide and Reduced Graphene Oxide. *Colloids Surf., B* **2012**, *89*, 79–85.
49. Yan, L.; Zhao, F.; Li, S.; Hu, Z.; Zhao, Y. Low-Toxic and Safe Nanomaterials by Surface-Chemical Design, Carbon Nanotubes, Fullerenes, Metallofullerenes, and Graphenes. *Nanoscale* **2011**, *3*, 362–382.
50. Mejias Carpio, I. E.; Santos, C. M.; Wei, X.; Rodrigues, D. F. Toxicity of a Polymer−Graphene Oxide Composite against Bacterial Planktonic Cells, Biofilms, and Mammalian Cells. *Nanoscale* **2012**, *4*, 4746–4756.
51. Yang, K.; Gong, H.; Shi, X.; Wan, J.; Zhang, Y.; Liu, Z. *In Vivo* Biodistribution and Toxicology of Functionalized Nano-Graphene Oxide in Mice after Oral and Intraperitoneal Administration. *Biomaterials* **2013**, *34*, 2787–2795.
52. Yang, K.; Feng, L.; Shi, X.; Liu, Z. Nano-Graphene in Biomedicine: Theranostic Applications. *Chem. Soc. Rev.* **2013**, *42*, 530–547.
53. Bitounis, D.; Ali-Boucetta, H.; Hong, B. H.; Min, D.; Kostarelos, K. Prospects and Challenges of Graphene in Biomedical Applications. *Adv. Mater.* **2013**, 10.1001/adma.201203700.